

Invited paper

Dane W. deQuilettes*, Madeleine Laitz, Roberto Brenes, Benjia Dou, Brandon T. Motes, Samuel D. Stranks, Henry J. Snaith, Vladimir Bulović and David S. Ginger

Maximizing the external radiative efficiency of hybrid perovskite solar cells

<https://doi.org/10.1515/pac-2019-0505>

Abstract: Despite rapid advancements in power conversion efficiency in the last decade, perovskite solar cells still perform below their thermodynamic efficiency limits. Non-radiative recombination, in particular, has limited the external radiative efficiency and open circuit voltage in the highest performing devices. We review the historical progress in enhancing perovskite external radiative efficiency and determine key strategies for reaching high optoelectronic quality. Specifically, we focus on non-radiative recombination within the perovskite layer and highlight novel approaches to reduce energy losses at interfaces and through parasitic absorption. By strategically targeting defects, it is likely that the next set of record-performing devices with ultra-low voltage losses will be achieved.

Keywords: 2018 IUPAC-Solvay Award; electroluminescence; non-radiative recombination; perovskite; photoluminescence; photovoltaics; solar energy; voltage loss.

Introduction

Photovoltaic (PV) devices and light-emitting diodes (LEDs) are important optoelectronic devices that are beginning to revolutionize renewable energy generation and increase energy efficiency [1]. Despite what appears to be opposite function – generation versus consumption of energy – the physical operation of PVs and LEDs is, in fact, complementary. Namely, the action of photon absorption and subsequent current collection is the reverse process of current injection followed by photon emission. Therefore, there is a direct link between photovoltaic quantum efficiency and electroluminescence (EL) efficiency as shown in the fundamental reciprocity relations derived by Rau, which establish that a solar cell performing near its theoretical limit will also be a highly luminescent LED [2, 3]. This understanding has driven the optimization of external radiative emission through reducing non-radiative loss channels, which has led to the record-performing,

Article note: A collection of peer-reviewed articles by the winners of the 2018 IUPAC-SOLVAY International Award for Young Chemists.

***Corresponding author: Dane W. deQuilettes,** Research Laboratory of Electronics, Massachusetts Institute of Technology, 77 Massachusetts Avenue, Cambridge, MA 02139, USA; and Department of Chemistry, University of Washington, Box 351700, Seattle, WA 98195-1700, USA, e-mail: danedeq@mit.edu

Madeleine Laitz, Roberto Brenes and Vladimir Bulović: Department of Electrical Engineering and Computer Science, Massachusetts Institute of Technology, 77 Massachusetts Avenue, Cambridge, MA 02139, USA; and Research Laboratory of Electronics, Massachusetts Institute of Technology, 77 Massachusetts Avenue, Cambridge, MA 02139, USA

Benjia Dou: Research Laboratory of Electronics, Massachusetts Institute of Technology, 77 Massachusetts Avenue, Cambridge, MA 02139, USA

Brandon T. Motes: Department of Electrical Engineering and Computer Science, Massachusetts Institute of Technology, 77 Massachusetts Avenue, Cambridge, MA 02139, USA

Samuel D. Stranks: Cavendish Laboratory, JJ Thomson Avenue, Cambridge CB3 0HE, UK

Henry J. Snaith: Department of Physics, University of Oxford, Clarendon Laboratory, Parks Road, Oxford OX1 3PU, UK

David S. Ginger: Department of Chemistry, University of Washington, Box 351700, Seattle, WA 98195-1700, USA

single-junction GaAs solar cells [4]. For GaAs, the optimization was straight-forward, as surface passivated materials had already demonstrated internal photoluminescence (PL) quantum efficiencies (η_{int}) as high as 99.7 %, and any residual loss resulted from parasitic absorption at the back contacts [4].

In contrast, the systematic optimization of perovskite power conversion efficiency (PCE) has been a challenge. In addition to minimizing non-radiative energy loss within the photoactive layer and at transport layer interfaces, perovskite PV performance also depends on reducing parasitic absorption in interlayers and at the metal contacts to harness photon recycling [5]. Quantifying and reducing losses from each of these mechanisms has been difficult considering the various compositions (i.e. ABX_3 where $\text{A}=\text{CH}_3\text{NH}_3^+$, $\text{HC}(\text{NH}_2)_2^+$, Cs^+ , Rb^+ ; $\text{B}=\text{Pb}^{2+}$, Sn^{2+} ; $\text{X}=\text{Cl}^-$, I^- , Br^-), transport layers (PCBM, TiO_2 , SnO_2 , Spiro-OMeTAD, PTAA, PEDOT:PSS), and metal contacts (Au, Ag, Al, Cu). Each chemical and architectural permutation results in unique defect densities and distributions throughout the device stack. Researchers have explored and continue to expand this wide parameter space with the goal of converging on a set of materials that maximizes absorption and minimizes overall non-radiative loss. This strategy can be effective for devices operating far below the theoretical performance limit, but is less effective for devices with $>20\%$ PCE, where each layer and interface must be globally optimized. Presently, a lack in understanding of how non-radiative loss is distributed throughout perovskite devices has limited typical PCEs to $\sim 20\%$ and open circuit voltages (V_{oc} s) to ~ 1.15 V, corresponding to a non-radiative voltage loss ($\Delta V_{\text{oc}}^{\text{nr}}$) of ~ 0.15 V (150 mV), which is defined as the radiative theoretical limit $V_{\text{oc}}, V_{\text{oc}}^{\text{rad}}$, minus the device V_{oc} (i.e. $\Delta V_{\text{oc}}^{\text{nr}} = V_{\text{oc}}^{\text{rad}} - V_{\text{oc}}$). In this review, we intentionally focus on $\Delta V_{\text{oc}}^{\text{nr}}$, which takes into account the real external response of the PV, as opposed to another commonly cited metric, voltage deficit ($W_{\text{oc}} = E_g - V_{\text{oc}}$), which is more prone to reporting error due to the various methods used to determine the optical bandgap (E_g) [6]. The next generation of high-efficiency perovskite PVs will need to consistently demonstrate $\Delta V_{\text{oc}}^{\text{nr}} < 0.10$ V to reach PCEs $>25\%$, which is feasible if recombination mechanisms are isolated, quantified, and reduced. We note that although this study highlights V_{oc} as a critical device parameter to optimize, recent analysis by Krückemeier et al. also suggests resistive losses as another key metric to improve performance [6].

In order to better understand non-radiative loss in perovskites, measurements of a solar cell run in reverse as an LED can complement measurements of PCE [7]. The external LED emission efficiency (Q_{LED}^e) is a practical figure of merit that quantifies the degree of non-radiative loss as well as how close a material is to its own thermodynamic (i.e. radiative) limit. Q_{LED}^e can easily be experimentally determined by measuring the emitted flux over the injected current (where $J_{\text{inj}} \sim J_{\text{sc}}$, the short-circuit current density of the PV). If not measured directly, an analogous value can also be calculated with the photovoltaic external quantum efficiency (EQE_{PV}) spectrum, measured at normal incidence, and the device V_{oc} using the reciprocity relations, which is often referred to as external radiative efficiency (ERE) as shown in eqs. 1 and 2 [8].

$$\text{ERE} = \frac{e^{(qV_{\text{oc}}/kT)} \int_{E_g} \text{EQE}_{\text{PV}}(E) \phi_{\text{BB}}(E) dE}{\int_{E_g} \text{EQE}_{\text{PV}}(E) \phi_{\text{AM1.5}}(E) dE} \quad (1)$$

$$= \frac{e^{(qV_{\text{oc}}/kT)} \cdot J_0^{\text{rad}}}{J_{\text{sc}}} \quad (2)$$

Where $\phi_{\text{BB}}(E)$ is the black body spectral photon flux of the solar cell at a temperature of T and $\phi_{\text{AM1.5}}(E)$ is the Air Mass 1.5, global-tilt solar irradiance spectrum.

Just as PCE is a function of J_{sc} , V_{oc} , and fill factor (FF); ERE is a function of J_{sc} , the dark saturation current density (J_0^{rad}), T , and the V_{oc} (see SI for assumptions).

The ability to experimentally measure and/or calculate the non-radiative loss for any device from standard PV measurements is a powerful tool. Therefore, we evaluate the ERE of perovskite devices over the past decade by using reported EQE spectra and V_{oc} values to track progress in reducing non-radiative loss. Figure 1a shows the ERE and $\Delta V_{\text{oc}}^{\text{nr}}$ of a selection of perovskite solar cell devices from pioneering papers as a function of publication date (see Table S1). The first demonstration of a perovskite solar cell in 2009 from Miyasaka and coworkers yielded a PCE of 3.8 % [9], with a corresponding ERE of 2.0×10^{-10} % and $\Delta V_{\text{oc}}^{\text{nr}}$ of 0.69 V. These values have significantly improved more recently, where record 23–25 % PCE devices have

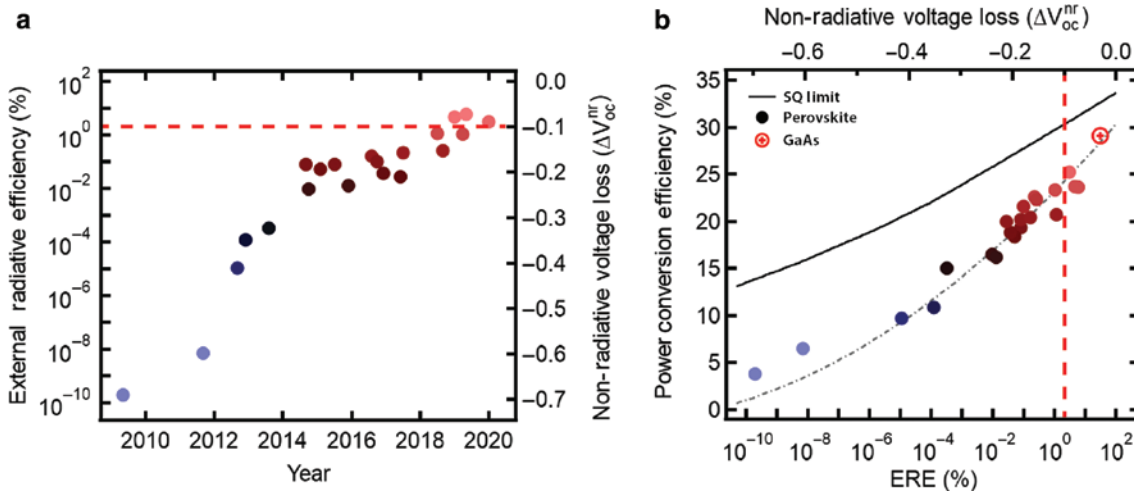


Fig. 1: (a) External radiative efficiency (ERE) and non-radiative voltage loss $\left(\Delta V_{oc}^{nr} = \frac{kT}{q} \ln(\text{ERE})\right)$ of a selection of pioneering perovskite device work as a function of publication date. The red dashed line represents the threshold for achieving the next set of high ERE and low ΔV_{oc}^{nr} devices. (b) Plot of perovskite power conversion efficiency (PCE) versus the ERE and ΔV_{oc}^{nr} along with a nonlinear trendline (dashed black line) and the record GaAs solar cell. The black solid line shows the Shockley-Queisser (SQ) maximum theoretical PCE irrespective of material bandgap.

demonstrated ERE values of $\sim 6\%$ ($\Delta V_{oc}^{nr} \sim 0.07$ V). We highlight the plateauing of ERE in the last few years, a trend often observed as materials approach their theoretical limits. In addition to tracking ERE over the years, Fig. 1b also shows the correlation of perovskite ERE with PCE plotted against the Shockley-Queisser (SQ) theoretical limit (black solid line, also see Fig. S1). As ERE approaches 100%, the gap between experimental PCE and the SQ radiative limit narrows. As a point of comparison to perovskite performance, Fig. 1b also shows the record GaAs solar cell fabricated by Alta Devices with a PCE of 29.1% and an ERE of 30.6%.

State-of-the-art perovskite solar cells only demonstrate ERE values $\sim 6\%$ and $\Delta V_{oc}^{nr} \sim 0.07$ V (c.f. Fig. 1) [12], suggesting that there is room for significant improvement in radiative efficiency. This critical review focuses on the progress made in identifying and eliminating non-radiative loss within the perovskite layer. Furthermore, we highlight advances made in interfacial passivation and describe the next steps toward reducing parasitic absorption and harnessing photon recycling in PV devices. We suggest additional experiments and analyses that could accelerate the optimization of ERE and the fabrication of perovskite devices with $\Delta V_{oc}^{nr} < 0.10$ V that could be competitive with record-setting GaAs solar cells (29%) [13]. Just as steady improvements in GaAs PV power output were enabled by systematic optimization of the ERE, perovskite PVs are also poised to significantly benefit from further reductions in non-radiative recombination and concomitant enhancements in ERE.

Bulk and surface non-radiative recombination

Apart from benchmarking device performance relative to theoretical limits, ERE or Q_{LED}^e serve as reference points for the sequential evaluation of isolated perovskite layers and multiple transport layers during the fabrication of a device. For example, similar to electroluminescence (EL), PL is a method capable of probing non-radiative recombination in photoactive layers without the need for contacts (see SI for comparison of reciprocity relations for PL versus EL). If the external PL quantum efficiency (η_{ext}) of a neat perovskite layer is 1%, it is unlikely that this photoactive layer would demonstrate a Q_{LED}^e efficiency $> 1\%$ in a PV device, due to additional non-radiative channels introduced from the deposition of interfacial layers. By comparing η_{ext} and Q_{LED}^e values through the device fabrication process by sequentially considering half and full device stacks, one can identify which layers and interfaces need to be further optimized.

Passivation steps during manufacturing have been critical for commercializing a wide range of semiconductors to date [16]. In perovskites, improvements in η_{ext} through the introduction of small passivating

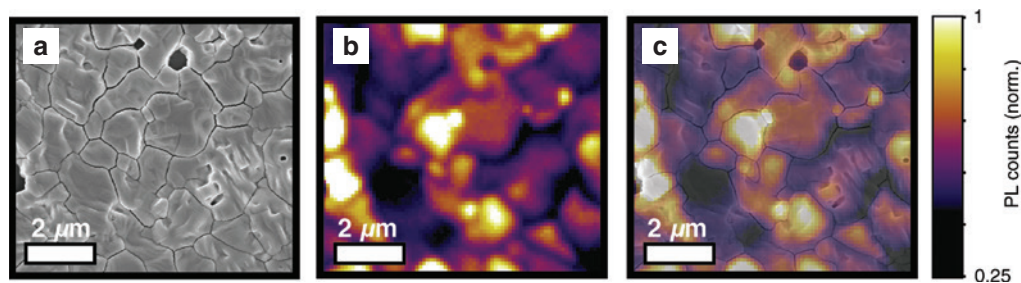


Fig. 2: (a) Correlated scanning electron microscopy (SEM) image, (b) fluorescence image, and (c) composite image of an unencapsulated $\text{CH}_3\text{NH}_3\text{PbI}_3(\text{Cl})$ thin film on glass showing significant variations in photoluminescence (PL) intensity across different grains and grain boundaries. Reprinted with permission from the American Association for the Advancement of Science [18].

molecules (i.e. pyridine) yielded early progress in reducing non-radiative recombination and improving PV device performance [14, 15]. Although effective, a fundamental understanding of the nature of the defects in perovskites and how they can be selectively targeted is still in its infancy. Accurately determining and reducing non-radiative centers in perovskites is further complicated by the morphology, as perovskite films self-assemble into nanostructured and polycrystalline materials, which are composed of a spatially varying ensemble of grains and grain boundaries with different compositions and defect distributions.

The use of conventional fluorescence microscopy, typically employed in biological systems [17], has also been applied to semiconductor research and provided a valuable platform to investigate the impact of microstructure on local energy loss. The extension of this tool to perovskite thin films has led to exciting new discoveries informing rational material design and has been leveraged to deploy targeted chemical passivation strategies leading to improved PCE.

Figure 2a shows a top-view scanning electron micrograph of a $\text{CH}_3\text{NH}_3\text{PbI}_3(\text{Cl})$ perovskite thin film with a correlated fluorescence image (Fig. 2b). This study revealed the spatial variation in non-radiative recombination rates and defect density, which has since been confirmed by several other studies [19–21]. The detrimental impact of defects at perovskite surfaces has been further highlighted by depth-dependent measurements of defect distributions using cathodoluminescence [22] and two-photon PL approaches [23–25]. We note that the analysis of emission images can be complicated and care must be taken to perform measurements at excitation fluences relevant to solar illumination conditions [21].

Spatial maps showing variations in the non-radiative recombination rate have provided critical information on how to strategically reduce defect concentrations and optimize η_{ext} . Briefly, we will review some of the advances made in reducing non-radiative recombination in metal halide perovskites. Specifically, we focus on characterization using fluorescence microscopy, which has facilitated the rapid evaluation of passivation strategies by simply studying PL maps before and after treatment.

Strategies to reduce non-radiative recombination

Light soaking

One promising strategy that was quickly identified was the improvement of film emission under continuous illumination and with different atmospheres (i.e. air, humidity, etc.) [26, 27]. Figure 3a shows a fluorescence image before exposing the film to simulated sunlight (100 mW/cm^2 , AM 1.5). The film initially exhibited significant heterogeneity in PL emission, consistent with Fig. 2, which became more homogeneous after light soaking (Fig. 3b). Dark grains with larger defect densities improved to a greater extent than grains initially exhibiting lower defect densities. We monitored the retention of these improvements by intermittently measuring the fluorescence map after time in the dark (Fig. 3c and d). Interestingly, after several hours in the

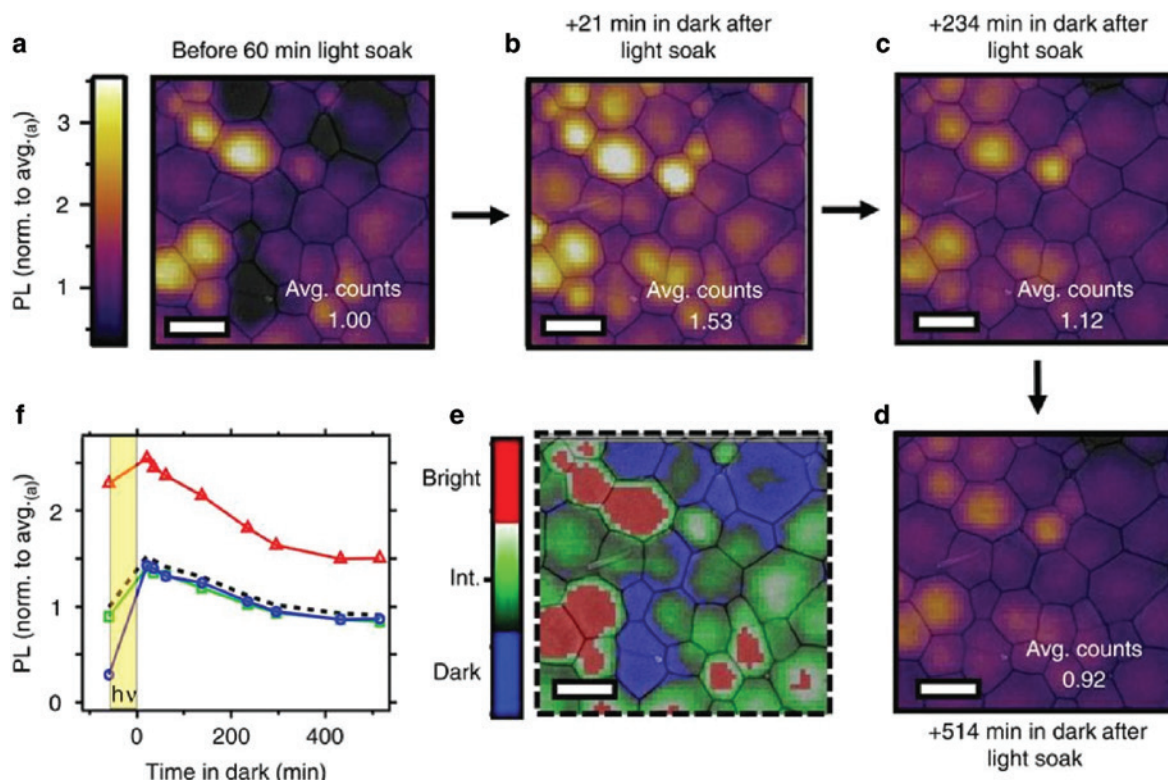


Fig. 3: Photoluminescence (PL) images of an unencapsulated $\text{CH}_3\text{NH}_3\text{PbI}_3$ thin film (with a hypophosphorous acid additive) on glass under pulsed excitation (470 nm, 40 MHz repetition rate, $0.03 \mu\text{J}/\text{cm}^2$ per pulse) measured in nitrogen with semitransparent scanning electron microscopy (SEM) images overlaid (a) before light soaking, and after exposing the entire film to simulated sunlight (AM 1.5, $100 \text{ mW}/\text{cm}^2$) for 60 min and leaving in the dark for (b) 21 (c) 234 and (d) 514 min (all images have the same PL intensity scale normalized to the average PL intensity in (a), scale bars, $1 \mu\text{m}$). (e) Three-color scale image showing the regions classified as dark, intermediate (Int.) and bright. (f) Local PL enhancement and relaxation for dark (blue, enhancement of $4.9\times$), intermediate (green, enhancement of $1.6\times$) and bright (red, enhancement of $1.1\times$) regions, where the time (t) under illumination is highlighted by the yellow shaded region for $-60 \leq t \leq 0$ min, and $t > 0$ show the local PL relaxation dynamics over time left in the dark. The dotted black line is the PL relaxation averaged across the whole fluorescence image. Reprinted with permission from Nature Publishing Group [26].

dark, a new equilibrium was reached (Fig. 3a vs. d) corresponding to a redistribution of emission intensities. Through the correlation of fluorescence images with time-of-flight secondary ion mass spectrometry (TOF-SIMS) measurements, we showed that this redistribution in emission intensities correlated with local iodide migration and subsequent passivation of defects.

Molecular post-deposition treatments for chemical passivation

In addition to decreasing defect density by light-soaking, chemical passivation utilizing Lewis Bases and electron donating moieties has also been highly effective. Noel et al. first demonstrated improvements in PL lifetime from ~ 350 ns to $\sim 2 \mu\text{s}$ after treatment with pyridine and thiophene, which corresponded to maximum η_{ext} values of $\sim 20\%$ at 1-sun equivalent carrier density (i.e. $\lambda_{\text{exc}} = 532$ nm, $60 \text{ mW}/\text{cm}^2$) [14]. Although pyridine treatments were promising, other molecules with higher selectivity had yet to be discovered. In this regard, we have reported a wide range of effective passivating agents including small thiols, phosphines, phosphine-oxides, and amines including ethanedithiol, octanethiol, octadecanethiol; triphenylphosphine (PPh₃); *n*-trioctylphosphine oxide (TOPO); butyl amine and tetramethylethylenediamine [28]. Other successful passivation strategies include carboxyl, phenethyl, fullerenes and their derivatives [29, 30], as well as Lewis acid-base adducts, which have recently been highlighted in a review by Aydin et al. [31].

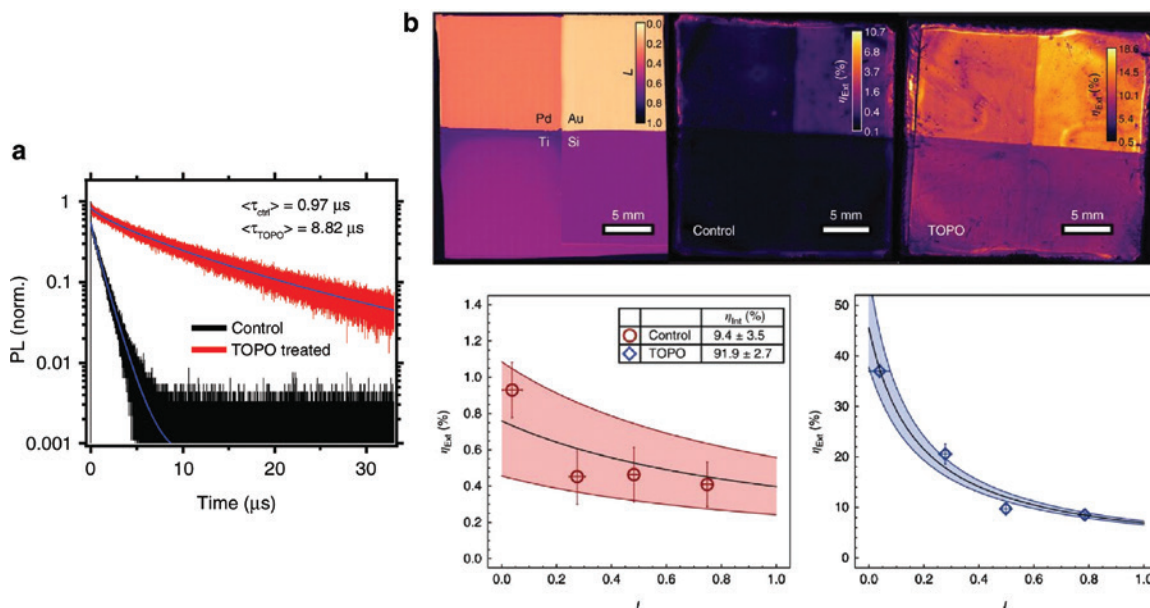


Fig. 4: (a) Champion bulk time-resolved photoluminescence (PL) decay traces of control (black) and *n*-trioctylphosphine oxide (TOPO, red) treated $\text{CH}_3\text{NH}_3\text{PbI}_3$ films on glass excited with pulsed excitation (470 nm, 30 kHz repetition rate, 50 nJ/cm^2 per pulse). (b) Spatial map showing measured optical loss factors, $L = 1 - \text{Reflectivity} = 1 - R$, of Au, Pd, Ti and Si quadrants of a metal back-reflector substrate before perovskite deposition. Spatial map showing η_{ext} for a typical control and TOPO-treated film deposited on the multi-metal back-reflector substrate. η_{ext} data as a function of L for a control film and champion TOPO-treated film, respectively. Error bars, shaded areas and black lines are 95% confidence intervals over the spatial heterogeneity in the data points, 95% confidence intervals of the nonlinear regression, and nonlinear regression fits, respectively. Adapted with permission from the American Chemical Society [28] and Nature Publishing Group [33].

Upon further mechanistic analysis of these electron-donating molecules, solid-state nuclear magnetic resonance (NMR) showed that they are primarily confined to the surface and form a new chemical bond likely with electron-deficient surface states (i.e. Pb^{2+}) [28]. Figure 4 shows time-resolved PL for a $\text{CH}_3\text{NH}_3\text{PbI}_3$ thin film before and after spin-coating a surface treatment of TOPO in chlorobenzene, where the PL lifetime improved from $\sim 1 \mu\text{s}$ to almost $9 \mu\text{s}$ ($\lambda_{\text{exc}} = 470 \text{ nm}$, 30 kHz repetition rate, 50 nJ/cm^2 per pulse). Figure 4b shows fluorescence images before and after TOPO treatment on a multi-metal substrate with varying back surface parasitic absorption. Using a method previously applied to high-quality GaAs [32], we determined η_{int} to be $91.9 \pm 2.7\%$ and the *quasi*-Fermi level splitting to be 1.28 eV, which is $\sim 97\%$ of the theoretical limit [33]. Importantly, these results show that the majority of non-radiative defect sites are located at the perovskite surfaces and can be effectively targeted with the judicious choice of passivating molecules.

These strategies have been directly applied to devices where TOPO passivation helped achieve a record Q_{LED}^e of 14.36% [34], which has been further improved to 20.1% with passivation using 4,9-dioxa-1,12-dodecanediamine (DDDA), 2,2'-[oxybis(ethylenoxy)]diethylamine (ODEA) [35]. TOPO has also served as a benchmark in fabricating PV devices with record high $V_{\text{oc,s}}$ of 1.26 V with a low $\Delta V_{\text{oc}}^{\text{nr}}$ of 0.0579 V [12].

Perovskite interfaces and contacts

With neat perovskite films now capable of reaching $\eta_{\text{int}} > 90\%$ and $\eta_{\text{ext}} \sim 50\%$ [36], the photoactive layer should no longer significantly limit PV performance. Subsequently, focus has shifted towards the optimization of interfaces and the reduction of parasitic absorption. Systematic analysis of voltage loss due to the introduction of interfaces has recently been studied by extracting the implied voltage through measurements of the *quasi*-Fermi level splitting using PL [37]. For example, Stolterfohl et al. used absolute intensity PL measurements to fit the high-energy tail of the PL spectrum, from which the implied V_{oc} of the perovskite film

Table 1: Perovskite formulations and passivation methods to achieve non-radiative voltage losses (ΔV_{oc}^{nr}) < 0.15 V.

Author	Architecture	Passivation	V_{oc} (V)	ΔV_{oc}^{nr} (V)	Percent of ERE (%) V_{oc}^{rad} (%)	
Liu et al. [12]	ITO/PTAA/MAPbI ₃ (Cl)/PCBM/BCP/Ag	PCBM Interface Engineering: toluene/CB solvent	1.26	0.0579	95.6	9.84
Jiang et al. [39]	ITO/SnO ₂ /FA _{1-x} MA _x PbI ₃ /Passivation/Spiro-OMeTAD/Au	Surface Passivation: phenylethylammonium iodide (PEAI)	1.18	0.0693	94.5	6.35
Yang et al. [30]	ITO/PTAA/Cs _{0.05} FA _{0.81} MA _{0.14} PbI _{2.55} Br _{0.45} (Passivation Additive)/C ₆₀ /BCP/Cu	Precursor Additive: D-4-tert-butylphenylalanine (D4TBP)	1.23	0.0762	94.2	4.85
Luo et al. [40]	ITO/PTAA/(FA _{0.95} PbI _{2.95}) _{0.85} (MAPbBr ₃) _{0.15} /PC ₆₁ BM/C ₆₀ /BCP/Cu	Surface Passivation: guanidinium bromide (GABr)	1.21	0.0846	93.5	3.51
Peng et al. [41]	FTO/c-In-TiO ₂ /m-TiO ₂ /PMMA-PCBM/Cs _{0.07} Rb _{0.03} FA _{0.765} MA _{0.135} PbI _{2.55} Br _{0.45} /PMMA/Spiro-OMeTAD/Au	Double-Sided Surface Passivation: poly(methyl methacrylate) (PMMA)	1.22	0.0912	93.0	2.71
Saliba et al. [42]	FTO/c-TiO ₂ /m-TiO ₂ /CsRbFAMAPbI _{3-x} Br _x /Spiro-OMeTAD/Au	Precursor Additive: Rb ⁺	1.24	0.0977	92.7	2.10
Jung et al. [43]	FTO/c-TiO ₂ /m-TiO ₂ /(FAPbI ₃) _{0.95} (MAPbBr ₃) _{0.05} /Passivation/P3HT/Au	Surface Passivation: <i>n</i> -hexyltrimethylammonium bromide	1.15	0.116	90.9	1.05
Yoo et al. [44]	FTO/c-TiO ₂ /m-TiO ₂ /(FAPbI ₃) _{0.92} (MAPbBr ₃) _{0.08} /Passivation/Spiro-OMeTAD/Au	Surface Passivation: <i>n</i> -hexylmethylammonium bromide	1.17	0.123	90.5	0.783
Li et al. [45]	ITO/PEDOT:PSS/(FASnI ₃) _{0.6} (MAPbI ₃) _{0.34} (MAPbBr ₃) _{0.06} /C ₆₀ /BCP/Ag	No Passivation	0.888	0.101	89.8	1.89
Tavakoli et al. [46]	FTO/c-TiO ₂ /m-TiO ₂ /CsFAMAPbI _{3-x} Br _x (ADAHI)/Spiro-OMeTAD/Au	Spiro-OMeTAD Interface Passivation: adamantylammonium iodide (ADAHI) added to HTL solution	1.185	0.1466	88.99	0.3178
Zheng et al. [47]	ITO/PTAA/FA _x MA _{1-x} Pb(Br _{1-x} I _x) ₃ /choline chloride/C ₆₀ /BCP/Cu	Surface Passivation: quaternary ammonium halides	1.15	0.146	88.8	0.331

ΔV_{oc}^{rad} is the radiative theoretical V_{oc} limit taking into account the external quantum efficiency spectrum and fitting the low-energy data to an Urbach tail [6]. The amount of significant figures in the table reflect the precision in the reported device metrics.

was extracted. The perovskite film on its own displayed the potential to reach 1.21 V, consistent with other studies for an unpassivated film [33]. Upon introducing the transport layers, the implied V_{oc} decreased to 1.12 V, indicating the formation of new non-radiative recombination channels at the interfaces. Importantly, the prediction of the implied V_{oc} from PL measurements corroborates the experimental V_{oc} of PVs fabricated from the same material [38]. This method was further utilized by Kirchartz and coworkers, where they optimized a perovskite/PCBM interface through solvent engineering of chlorobenzene and toluene leading to a record V_{oc} of 1.26 V and ΔV_{oc}^{nr} of 0.0579 V (i.e. 95.6 % of the radiative theoretical V_{oc} limit) [12]. Other low ΔV_{oc}^{nr} s have been reported by Jiang et al. where they treated the perovskite surface with phenethylammonium iodide (PEAI) which resulted in a ΔV_{oc}^{nr} of 0.0693 V [39]. Table 1 shows, to the best of our knowledge, a list of the lowest ΔV_{oc}^{nr} devices along with the passivation strategy deployed to reduce non-radiative recombination. The majority of low ΔV_{oc}^{nr} devices were achieved either through a surface treatment or interface modification, although perovskite precursor additives as well as 2D perovskite surface passivation are also effective approaches [31].

Photon recycling

Once the perovskite optoelectronic quality has been roughly optimized ($\eta_{int} > 50\%$, $\eta_{ext} > 10\%$) and interfacial recombination has been reduced, a phenomenon known as photon recycling can be exploited. Photon recy-

cling is the reabsorption of photons generated and waveguided within the film following a radiative recombination event. Due to the large index of refraction mismatch between the perovskite absorber film ($n \sim 2.6$) and the surrounding environment, there is a relatively low photon escape probability ($\sim 5\%$) [33]. Under constant illumination, photon recycling leads to an increase in both the steady-state photon and carrier densities, and the trapping of internally emitted photons reduces the rate of externally emitted photons (i.e. the radiative saturation current, J_0^{rad}) [11]. The enhanced steady-state carrier density leads to a larger *quasi*-Fermi level splitting and voltage, while the multiple absorption and emission events within the film allow for Q_{LED}^e to exceed the intrinsic material escape probability. Indeed, state-of-the-art PV devices have demonstrated Q_{LED}^e and ERE values exceeding 5% [39]. With efficient photon recycling, it is thus possible to observe both enhanced steady-state carrier density and η_{ext} [11].

Photon recycling can be effectively utilized by reducing non-radiative recombination and parasitic absorption at metal contacts. For GaAs, changes in electrode reflectivity from 80% to 100%, were predicted to lead to a voltage enhancement from 1.104 to 1.145 V [3]. In fact, in perovskites, photon recycling must be present to reach $\Delta V_{\text{oc}}^{\text{nr}} < 0.07$ V [5, 11]. For high-quality perovskite samples and optimized interfaces, significant gains in the voltage at maximum-power-point and V_{oc} can be achieved by reducing the extent of parasitic absorption within the device stack and engineering highly reflective back-contacts to harness photon recycling [3], as previously done in GaAs [48].

Conclusions

The external radiative efficiency (ERE) is a useful metric in assessing the progress of a photovoltaic (PV) technology in addition to power conversion efficiency (PCE). Specifically, the ERE value reveals the degree of non-radiative loss within the device stack and can be used as a quantitative metric to compare different technologies on the same thermodynamic scale. For example, perovskites have now demonstrated ERE values as high as $\sim 6\%$, corresponding to PCEs of 23–25%, compared to GaAs which has demonstrated an ERE of 30.6% with a PCE of 29.1%. Looking forward, there are several loss pathways reducing photovoltages and EREs below their thermodynamic limits which can be mitigated by targeting defects. We reviewed recent advances towards identifying bulk and surface recombination within the perovskite layer as well as interfacial recombination. Both electroluminescence (EL) and photoluminescence (PL) serve as readily accessible characterization tools capable of quantifying non-radiative loss throughout the device stack. The highest voltage devices typically benefit from a thin passivating layer between the perovskite and transport layers. These devices have led to non-radiative voltage losses, $\Delta V_{\text{oc}}^{\text{nr}}$ s, of less than 0.07 V, which corresponds to values as high as $\sim 95\%$ of the radiative theoretical V_{oc} limit. Ultimately, both reducing non-radiative recombination through defect management and engineering architectures that exploit photon recycling will push PV device voltages and LED performance towards theoretical limits.

Acknowledgements: D.W.D, M.L., R.B., B.D., B.M., and V.B. acknowledge support for writing this critical review through the MIT-Tata GridEdge Solar Research Program, which is funded by the Tata Trusts. M.L. and R.B. acknowledge support from the National Science Foundation Graduate Research Fellowship under Grant No. (funder id: <http://dx.doi.org/10.13039/100000001>, 1122374). SDS acknowledges the Royal Society and Tata Group (funder id: <http://dx.doi.org/10.13039/501100000288>, UF150033). D.S.G. acknowledges DOE BES, (funder id: <http://dx.doi.org/10.13039/100000015>, DE-SC0013957) for supporting the early confocal microscopy work, as well as support of institutional, intellectual, and human resources built up over the years from the Office of Naval Research (ONR) photovoltaics program and current award (funder id: <http://dx.doi.org/10.13039/100000006>, N00014-17-1-2201). The authors thank Anurag Panda for valuable discussions as well as Deying Luo (Peking University), Zhiwei Liu (Peking University), and Chen Qi (University of California, Los Angeles) for providing external quantum efficiency data in references [40, 49, 50], respectively.

References

- [1] W. Zhang, G. E. Eperon, H. J. Snaith. *Nat. Energy* **1**, 16048 (2016).
- [2] U. Rau. *Phys. Rev. B* **76**, 085303 (2007).
- [3] O. D. Miller, E. Yablonovitch, S. R. Kurtz. *IEEE J. Photovolt.* **2**, 303 (2012).
- [4] E. M. Yablonovitch, D. Owen, S. R. Kurtz. *38th IEEE Photovoltaic Specialists Conference* **13055419**, 001556 (2012).
- [5] T. Kirchartz, F. Staub, U. Rau. *ACS Energy Lett.* **1**, 731 (2016).
- [6] L. Krückemeier, U. Rau, M. Stollerfoht, T. Kirchartz. *Adv. Energy Mater.* **10**, 1 (2019).
- [7] U. Rau, U. W. Paetzold, T. Kirchartz. *Phys. Rev. B* **90**, 3 (2014).
- [8] M. A. Green. *Prog. Photovolt: Res. Appl.* **20**, 472 (2012).
- [9] A. Kojima, K. Teshima, Y. Shirai, T. Miyasaka. *J. Am. Chem. Soc.* **131**, 6050 (2009).
- [10] L. M. Pazos-Outon, T. P. Xiao, E. Yablonovitch. *J. Phys. Chem. Lett.* **9**, 1703 (2018).
- [11] R. Brenes, M. Laitz, J. Jean, D. W. deQuilettes, V. Bulović. *Phys. Rev. Appl.* **12**, 014017 (2019).
- [12] Z. Liu, L. Krückemeier, B. Krogmeier, B. Klingebiel, J. A. Márquez, S. Levchenko, S. Öz, S. Mathur, U. Rau, T. Unold, T. Kirchartz. *ACS Energy Lett.* **4**, 110 (2018).
- [13] M. A. Green, Y. Hishikawa, E. D. Dunlop, D. H. Levi, J. Hohl-Ebinger, M. Yoshita, A. W. Y. Ho-Baillie. *Prog. Photovolt: Res. Appl.* **27**, 3 (2019).
- [14] N. K. Noel, A. Abate, S. D. Stranks, E. S. Parrott, V. M. Burlakov, A. Goriely, H. J. Snaith. *ACS Nano*. **8**, 9815 (2014).
- [15] A. Abate, M. Saliba, D. J. Hollman, S. D. Stranks, K. Wojciechowski, R. Avolio, G. Grancini, A. Petrozza, H. J. Snaith. *Nano Lett.* **14**, 3247 (2014).
- [16] A. G. Aberle. *Prog. Photovolt: Res. Appl.* **8**, 473 (2000).
- [17] K. Suhling, P. M. French, D. Phillips. *Photochem. Photobiol. Sci.* **4**, 13 (2005).
- [18] D. W. deQuilettes, S. M. Vorpahl, S. D. Stranks, H. Nagaoka, G. E. Eperon, M. E. Ziffer, H. J. Snaith, D. S. Ginger. *Science* **348**, 683 (2015).
- [19] M. Vrućinić, C. Matthiesen, A. Sadhanala, G. Divitini, S. Cacovich, S. E. Dutton, C. Ducati, M. Atatüre, H. Snaith, R. H. Friend, H. Sirringhaus, F. Deschler. *Adv. Sci.* **2**, 1500136 (2015).
- [20] S. Draguta, S. Thakur, Y. V. Morozov, Y. Wang, J. S. Manser, P. V. Kamat, M. Kuno. *J. Phys. Chem. Lett.* **7**, 715 (2016).
- [21] D. W. deQuilettes, S. Jariwala, S. Burke, M. E. Ziffer, J. T. Wang, H. J. Snaith, D. S. Ginger. *ACS Nano* **11**, 11488 (2017).
- [22] C. G. Bischak, E. M. Sanehira, J. T. Precht, J. M. Luther, N. S. Ginsberg. *Nano Lett.* **15**, 4799 (2015).
- [23] Y. Yang, M. Yang, D. T. Moore, Y. Yan, E. M. Miller, K. Zhu, M. C. Beard. *Nat. Energy* **2**, 16207 (2017).
- [24] C. Stavrakas, A. A. Zhumekenov, R. Brenes, M. Abdi-Jalebi, V. Bulovic, O. M. Bakr, E. S. Barnard, S. D. Stranks. *Energy Environ. Sci.* **11**, 2846 (2018).
- [25] Y. Yamada, T. Yamada, L. Q. Phuong, N. Maruyama, H. Nishimura, A. Wakamiya, Y. Murata, Y. Kanemitsu. *J. Am. Chem. Soc.* **137**, 10456 (2015).
- [26] D. W. deQuilettes, W. Zhang, V. M. Burlakov, D. J. Graham, T. Leijtens, A. Osherov, V. Bulovic, H. J. Snaith, D. S. Ginger, S. D. Stranks. *Nat. Commun.* **7**, 11683 (2016).
- [27] Y. Tian, M. Peter, E. L. Unger, M. Abdellah, K. Zheng, T. Pullerits, A. Yartsev, V. Sundstrom, I. Scheblykin. *Phys. Chem. Chem. Phys.* **17**, 24978 (2015).
- [28] D. W. deQuilettes, S. Koch, S. Burke, R. K. Paranjli, A. J. Shropshire, M. E. Ziffer, D. S. Ginger. *ACS Energy Lett.* **1**, 438 (2016).
- [29] Y. Shao, Z. Xiao, C. Bi, Y. Yuan, J. Huang. *Nat. Commun.* **5**, 5784 (2014).
- [30] S. Yang, J. Dai, Z. Yu, Y. Shao, Y. Zhou, X. Xiao, X. C. Zeng, J. Huang. *J. Am. Chem. Soc.* **141**, 5781 (2019).
- [31] E. Aydin, M. De Bastiani, S. De Wolf. *Adv. Mater.* **31**, 1900428 (2019).
- [32] Gmitter, I. S. E. Y. C. C. A. E. T. J. *Appl. Phys. Lett.* **62**, 131 (1993).
- [33] I. L. Braly, D. W. deQuilettes, L. M. Pazos-Outon, S. Burke, M. E. Ziffer, D. S. Ginger, H. W. Hillhouse. *Nat. Photonics* **12**, 355 (2018).
- [34] X. Yang, X. Zhang, J. Deng, Z. Chu, Q. Jiang, J. Meng, P. Wang, L. Zhang, Z. Yin, J. You. *Nat. Commun.* **9**, 1169 (2018).
- [35] W. Xu, Q. Hu, S. Bai, C. Bao, Y. Miao, Z. Yuan, T. Borzda, A. J. Barker, E. Tyukalova, Z. Hu, M. Kawecki, H. Wang, Z. Yan, X. Liu, X. Shi, K. Uvdal, M. Fahlman, W. Zhang, M. Duchamp, J. -M. Liu, A. Petrozza, J. Wang, L.-M. Liu, W. Huang, F. Gao. *Nat. Photon.* **13**, 418 (2019).
- [36] M. Abdi-Jalebi, Z. Andaji-Garmaroudi, S. Cacovich, C. Stavrakas, B. Philippe, J. M. Richter, M. Alsari, E. P. Booker, E. M. Hutter, A. J. Pearson, S. Lilliu, T. J. Savenije, H. Rensmo, G. Divitini, C. Ducati, R. H. Friend, S. D. Stranks. *Nature* **555**, 497 (2018).
- [37] V. Sarritzu, N. Sestu, D. Marongiu, X. Chang, S. Masi, A. Rizzo, S. Colella, F. Quochi, M. Saba, A. Mura, G. Bongiovanni. *Sci. Rep.* **7**, 44629 (2017).
- [38] M. Stollerfoht, C. M. Wolff, J. A. Márquez, S. Zhang, C. J. Hages, D. Rothhardt, S. Albrecht, P. L. Burn, P. Meredith, T. Unold, D. Neher. *Nat. Energy* **3**, 847 (2018).
- [39] Q. Jiang, Y. Zhao, X. Zhang, X. Yang, Y. Chen, Z. Chu, Q. Ye, X. Li, Z. Yin, J. You. *Nat. Photon.* **13**, 460 (2019).
- [40] D. Luo, W. Yang, Z. Wang, A. Sadhanala, Q. Hu, R. Su, R. Shivanna, G. F. Trindade, J. F. Watts, Z. Xu, T. Liu, K. Chen, F. Ye, P. Wu, L. Zhao, J. Wu, Y. Tu, Y. Zhang, X. Yang, W. Zhang, R. H. Friend, Q. Gong, H. J. Snaith, R. Zhu. *Science* **360**, 1442 (2018).

- [41] J. Peng, J. I. Khan, W. Liu, E. Ugur, T. Duong, Y. Wu, H. Shen, K. Wang, H. Dang, E. Aydin, X. Yang, Y. Wan, K. J. Weber, K. R. Catchpole, F. Laquai, S. De Wolf, T. P. White. *Adv. Energy Mater.* **8**, 1801208 (2018).
- [42] M. Saliba, T. Matsui, K. Domanski, J. Y. Seo, A. Ummadisingu, S. M. Zakeeruddin, J. P. Correa-Baena, W. R. Tress, A. Abate, A. Hagfeldt, M. Gratzel. *Science* **354**, 206 (2016).
- [43] E. H. Jung, N. J. Jeon, E. Y. Park, C. S. Moon, T. J. Shin, T. Y. Yang, J. H. Noh, J. Seo. *Nature* **567**, 511 (2019).
- [44] J. J. Yoo, S. Wieghold, M. C. Sponseller, M. R. Chua, S. N. Bertram, N. T. P. Hartono, J. S. Tresback, E. C. Hansen, J.-P. Correa-Baena, V. Bulović, T. Buonassisi, S. S. Shin, M. G. Bawendi. *Energy Environ. Sci.* **12**, 2192 (2019).
- [45] C. Li, Z. Song, D. Zhao, C. Xiao, B. Subedi, N. Shrestha, M. M. Junda, C. Wang, C.-S. Jiang, M. Al-Jassim, R. J. Ellingson, N. J. Podraza, K. Zhu, Y. Yan. *Adv. Energy Mater.* **9**, 1803135 (2019).
- [46] M. M. Tavakoli, W. Tress, J. V. Milić, D. Kubicki, L. Emsley, M. Grätzel. *Energy Environ. Sci.* **11**, 3310 (2018).
- [47] X. Zheng, B. Chen, J. Dai, Y. Fang, Y. Bai, Y. Lin, H. Wei, X. C. Zeng, J. Huang. *Nat. Energy* **2**, 17102 (2017).
- [48] B. M. Kayes, H. Nie, R. Twist, S. G. Spruytte, F. Reinhardt, I. C. Kizilyalli, G. S. Higashi. *37th IEEE Photovoltaic Specialists Conference*, 000004-000008 (2011).
- [49] S. Ye, H. Rao, Z. Zhao, L. Zhang, H. Bao, W. Sun, Y. Li, F. Gu, J. Wang, Z. Liu, Z. Bian, C. Huang. *J. Am. Chem. Soc.* **139**, 7504 (2017).
- [50] H. Zhou, Q. Chen, G. Li, S. Luo, T. B. Song, H. S. Duan, Z. Hong, J. You, Y. Liu, Y. Yang. *Science* **345**, 542 (2014).

Supplementary Material: The online version of this article offers supplementary material (<https://doi.org/10.1515/pac-2019-0505>).